ADVANCED MATERIALS

DOI: 10.1002/adma.200700309

A Bit per Particle: Electrostatic Assembly of CdSe Quantum Dots as Memory Elements**

By *Bikas C. Das*, *Sudip K. Batabyal*, and *Amlan J. Pal**

Semiconducting nanostructures exhibit attractive electrical, optical, and magnetic properties that are different from those of their bulk phase. Quantum dots, being quasi-zero-dimensional, have a sharper density of states than higher-dimensional structures. They hence have superior transport and optical properties and are thus suitable for various electronic and optoelectronic applications.[1–3] Because such properties are size-dependent, it is customary to vary the size of the particles to monitor device characteristics for novel applications. In recent years, gold and semiconducting nanoparticles, embedded in polymer matrices, exhibited electrical bistability for memory applications.[4–7] Electric-field-induced charge transfer followed by charge confinement in nanoparticles led to a high-conducting state. Device dimensions (thickness ranging from 50 nm to a couple of hundred of nanometers), however, restricted the use of these nanoparticles in high-density memory elements.

A two-dimensional array of nanoparticles can be achieved with the advent of layer-by-layer (LbL) electrostatic assembly.[7–9] In LbL films, the nanoparticles are electrostatically adsorbed because of suitable functional groups present in the stabilizer. They hence form a two-dimensional assembly. In such two-dimensional arrays, the properties of a single particle or dot (or an assembly of them) can be studied. In this article, we present our in-depth work on the electrical bistability in two-dimensional arrays of CdSe nanoparticles (with particles sizes ranging down to the quantum dot regime) in achieving *a bit per particle*.

The composition of the nanoparticles was evaluated by using X-ray diffraction (XRD), and high-resolution transmission electron microscopy (HRTEM) images; their sizes were measured from TEM images and electronic absorption spectra. XRD spectra showed diffraction patterns corresponding to CdSe crystals (Supporting Information, Fig. S1). HRTEM images of the nanoparticles showed lattice spacing corresponding to CdSe crystals, confirming the formation of CdSe nanoparticles (Supporting Information, Fig. S2). Infrared absorption spectra of the mercaptoacetic acid-capped particles showed the presence of vibrations corresponding to the ligands attached to the nanoparticles (Supporting Information, Fig. S3). TEM images of the nanoparticles, adsorbed on carbon-coated grids, showed nearly spherical particles (Supporting Information, Fig. S2). Scanning electron microscopy (SEM) images of the nanoparticles electrostatically adsorbed on a Si substrate show that the substrate was covered uniformly with the nanoparticles (Supporting Information, Fig. S4).

UV-vis electronic absorption spectra of four different CdSe nanoparticles dispersed in water are shown in Figure 1a. Each of the spectra shows a single peak. The peak wavelengths for the four nanoparticles is 372, 418, 474, and 508 nm, as is also evidenced by a photograph of the solutions (inset of Fig. 1a). The wavelengths correspond to a particle size of 3.5, 4.6, 6.7, and 8.7 nm for CdSe. In other words, larger CdSe particles have a smaller band gap. The sizes were obtained from the equation[10]

$$R = \frac{h}{E_{gn} - E_{gb}} \sqrt{\left[\frac{E_{gb}}{2m^*}\right]} \quad (1)$$

where R is the particle size, h is the Plank constant, m^* is the effective mass of the electron ($= 0.1 \times$ the rest mass of the electron), and E_{gb} and E_{gn} are the band gaps for the bulk ($= 1.84$ eV) and nanoparticles, respectively. The size of the CdSe nanoparticles hence ranges down to the quantum dot regime.

We recorded the electronic absorption spectrum of a monolayer of CdSe nanoparticles on a quartz substrate. Because the value of absorbance was low for a monolayer, we confirmed deposition of the particles by monitoring the progress of the electrostatic adsorption process (LbL deposition) during multilayer deposition. For the 4.6 nm particles, electronic absorption spectra of a different number of layers of LbL films are shown in Figure 1b. All the five spectra showed a peak at 439 nm—the intensity of the band increasing with the number of layers deposited. The absorption band is red-shifted compared to that measured for 4.6 nm particles in dispersed solution. Because the 439 nm band corresponds to a particle size of 5.3 nm, which is not an integer multiple of 4.6 nm, the red-shift in the absorption spectrum cannot be caused by the formation of clusters in the films. The shift

[*] Prof. A. J. Pal, B. C. Das, S. K. Batabyal
Indian Association for the Cultivation of Science
Department of Solid State Physics
Kolkata 700032 (India)
E-mail: sspajp@iacs.res.in

[**] BCD acknowledges a CSIR Junior Research Fellowship No. 9/80(504)/2006-EMR-I, Roll No. 503982. The Department of Science and Technology of the Government of India financially supported the work through a Ramanna Fellowship SR/S2/RFCMP-02/2005. Supporting Information is available online from Wiley InterScience or from the author.

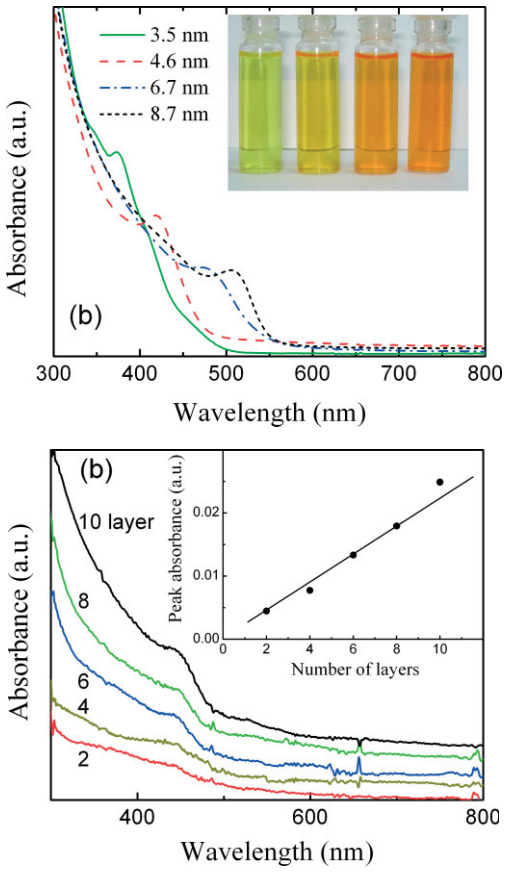

Figure 1. The electronic absorption spectra of CdSe nanoparticles. a) CdSe nanoparticles of different sizes in dispersed solution (the inset shows photograph of the solutions). b) LbL films of 4.6 nm CdSe nanoparticles. Number of layers of the LbL film is shown in the figure. The inset shows absorbance at 439 nm as a function of the number of layers. The results show that different sized nanoparticles were fabricated and successfully deposited on a substrate by the LbL film-deposition procedure.

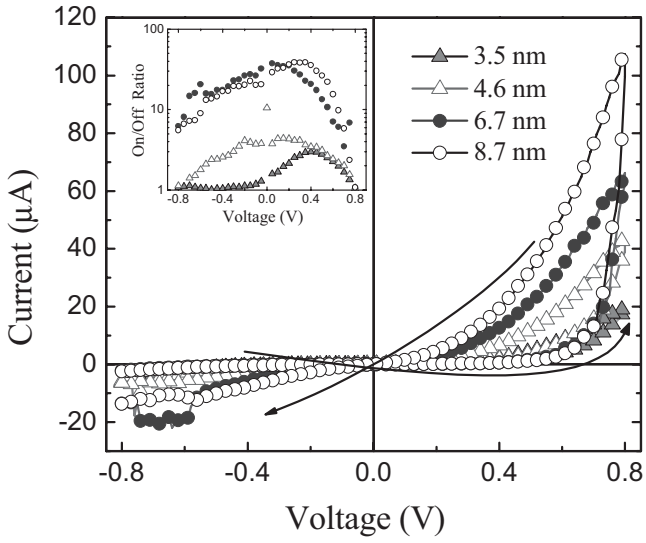

Figure 2. *I–V* characteristics of the CdSe monolayer. The *I–V* characteristics depend on the sweep direction (shown by arrows). A positive voltage induces a higher current during the voltage sweep. By changing the particle size, the on/off ratio (the current and voltage of both sweep directions) changes. The inset shows a plot of the on/off ratio as a function of voltage for the four nanoparticles. The size of the nanoparticles is shown in the legend.

could be due to the interaction between $-COO^-$ and $-NH_3^+$ groups on the surfaces of CdSe and the polycation, respectively, in LbL films. A restricted geometry in the LbL film might also result in the shift. The inset of Figure 1b shows the absorbance of the films at 439 nm as a function of the number of CdSe layers. A linear plot through the origin confirms that the CdSe nanoparticles were adsorbed uniformly during deposition of each and every layer.

Because LbL film deposition relies on electrostatic adsorption process with surface charge reversal during deposition of every layer, deposition of a monolayer is assured with a formation of a two-dimensional assembly. Moreover, because of the electrostatic interaction between the monolayer and the substrate, the top-electrode would not peel the monolayer off the substrate. Current–voltage (*I–V*) characteristics of different monolayer films were recorded with Hg as the top electrode. Voltage was swept in both bias directions. This in effect resulted in the application of a positive or negative voltage pulse before the voltage sweep. Results presented in Figure 2 for the four sizes of nanoparticles show that each of the monolayers exhibit electrical bistability. The bistability is prominent in the forward bias direction; current at a voltage during the two sweeps differs up to 40 times. The high-state current depends on the diameter of the nanoparticles. This could be due to lower barrier heights with the electrodes in larger particles, which have a lower band gap. With an increase in the diameter, the ratio between the current in the two states (the on/off ratio) also increased. This evidenced the size-dependent electrical bistability (inset of Fig. 2). The voltage required to achieve the high state, however, does not depend on the size of the particle. In all four cases, the current through the particles switched to a high value at a positive bias. The high-conducting state was retained during the whole sweep from a positive to a negative voltage, at which the current switched to a low magnitude. The electrical bistability was reversible, that is, when bias was applied in multiple loops, the *I–V* plot retraced itself in both sweep-directions (Supporting Information, Fig. S5). Electrical bistability was observed when the bias was swept to different voltages (Supporting Information, Fig. S6). The *I–V* characteristics were independent of the voltage scan-rate excluding any role of ion migration. The *I–V* characteristics measured at different points on the film were almost identical in nature showing a high degree of reproducibility (Supporting Information, Fig. S7). The low degree of variation could be due to the different sizes of Hg blobs used at different times. The *I–V* characteristics were however nonlinear in both bias directions. Such non-ohmic behavior could be due to different interfaces in the metal–semiconductor–metal structures. In all the cases, the current was lower than

ADVANCED MATERIALS

that in measurements with a direct contact between indium tin oxide (ITO) and Hg. Such a reproducible bistability was observed even when the size of the nanoparticles was in the quantum dot regime.

It is important to demonstrate that the electrical bistability and memory phenomenon are observed not only in a large area of a two-dimensional array but also in a nanoscale regime. With the aim of achieving a bit per particle or a truly nanoscale memory element, the array of the nanoparticles was characterized also by a scanning tunneling microscope tip. The two-dimensional array, deposited on a highly-doped Si wafer, was mapped. Although the bare wafer showed a complete absence of any morphology, nanoparticles were clearly visible in the topography of the array on the wafers (Fig. 3a and b, respectively). The size of the nanoparticles matched the value obtained from the HRTEM image. With the scanning tunneling microscope tip placed on one of the particles, we recorded the *I–V* characteristics after the application of suitable voltage pulses. Figure 3c and d represent voltage scans towards a negative and a positive voltage, respectively. In each of the cases, three scans, namely i) an initial one, ii) after application of a +6 V pulse, and iii) after a –6 V pulse, are shown. Figure 3c and d shows that the +6 V pulse switches the conductivity of the particle, as evidenced by the higher current (at any voltage) during the voltage scan as compared to the *I–V* characteristics before the application of the +6 V pulse. The switching is reversible; the initial conducting state is re-attainable by the application of a reverse-voltage pulse. Switching between the two bistable states is almost identical in both voltage-scan directions (Fig. 3c and d). Measurements were carried out at different points and also when +6 and –6 V pulses were applied in cycles. The *I–V* characteristics after the respective pulses are reproducible. In effect, with the +6 V pulse we can "write" the high state. The –6 V pulse "erases" the high state and reinstates the initial low-conducting state. With the *I–V* scans after +6 and –6 V pulses, we "read" the state of the device. The current at any voltage during the read scans differed displaying memory phenomenon. Such measurements on a two-dimensional array of nanoparticles demonstrate memory elements with a density of *a bit per particle*. Because the size of the CdSe nanoparticles ranges down to the quantum dot regime, the results demonstrate quantum dots as memory elements. As control experiments, we recorded *I–V* characteristics between Si and the scanning tunneling microscope tip. The *I–V* characteristics due to 1–1.5 nm native SiO_2 on Si were symmetric. Current through the nanoparticles was always less than the current measured without a nanoparticle monolayer. The current measured for a poly(allylamine hydrochloride) (PAH) monolayer only did not yield any bistability. Particles adsorbed on highly ordered pyrolytic graphite (HOPG) also showed similar conductance switching. It is worthwhile to mention that monolayers of other nanoparticles, such as PbS, CdS, and so on, also exhibited such a bistability—the on/off ratio being dependent on the material of the nanoparticles.

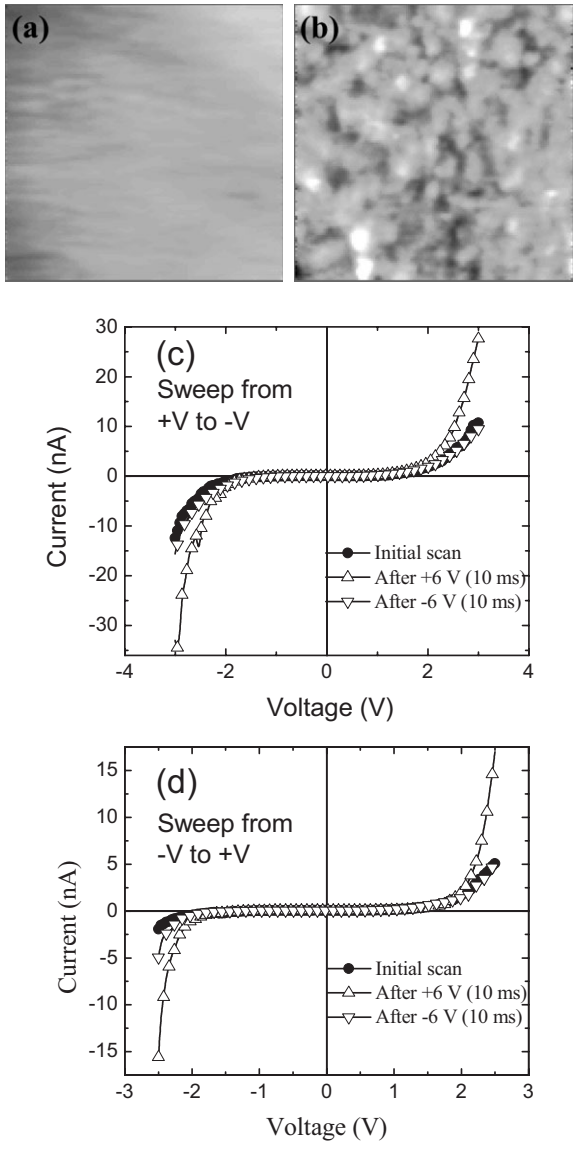

Figure 3. Scanning tunneling microscopy image and *I–V* characteristics of a monolayer with a Pt/Ir-tipped scanning tunneling microscope. The topography of a) bare silicon (18 nm × 18 nm image) and b) a monolayer of CdSe nanoparticles (28 nm × 28 nm image) show the presence of nanoparticles on the wafer. The diameter of a particle is 3.5 nm. *I–V* characteristics of the pristine nanoparticle (off state), after switching to a high state (on state), and after reinstating the low-conducting off state are shown in (c) and (d). The characteristics of the voltage-sweep in the forward- and reverse-bias directions are identical.

We calculated the normalized differential conductance of different nanoparticles as a function of tip voltage. With a decrease in size of the particles, the band gap obtained from the normalized conductance spectrum increased, supporting the results obtained from the electronic absorption spectra. From the differential conductance spectra, electrical bistability in nanoparticles can be explained in terms of charge confinement in the particles. By applying a suitable positive voltage pulse, the nanoparticles trap carriers and confine them. This is

evidenced in an increase in the local density of states calculated from the *I–V* characteristics (Fig. 4). Here, the d*I*/d*V* spectrum can be related to the local density of states, which are tuned by the voltage, and provide information on the surface states where conduction occurs. The decrease in the band

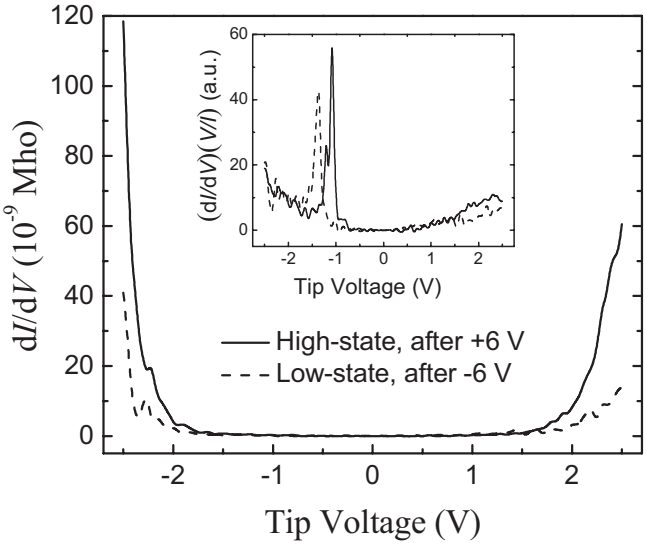

Figure 4. Differential conductance–voltage characteristics of a monolayer of CdSe nanoparticles in their high- and low-conducting states. The inset shows normalized conductance for the two states evidencing a decrease in the band gap upon switching. Conductance is calculated from the results presented in Figure 3.

gap upon switching to a high state can be observed in the normalized differential conductance versus voltage plot (inset of Fig. 4). At a suitable reverse bias, the confined carriers become detrapped to reinstate the pristine low-conducting state. The differential conductance further increases (and the band gap decreases) with the amplitude of voltage pulse that induces the high state. The results hence show that after application of a positive voltage pulse, surface conduction takes place through the nanoparticles resulting in the high-conducting state. Carriers, even if trapped at the capping (organic) layer, could hence change the conductivity of the nanoparticles to yield the high state.

To estimate the retention time of the states after inducing a high- and a low-conducting state, we probed them continuously by applying a small read voltage (Fig. 5). Here a +0.8 V and –0.8 V pulse (10 s) induced the respective states, while 0.3 V acted as the read pulse. The duty cycle of the read pulse was low, so that the interference of the read pulse on the induced state was as little as possible. The figure shows that the current under the probe voltage for the high-conducting state was much higher than the current when the low state was probed by the same voltage. The results show that the nanoparticles retained a state (that was written) for more than thirty minutes.

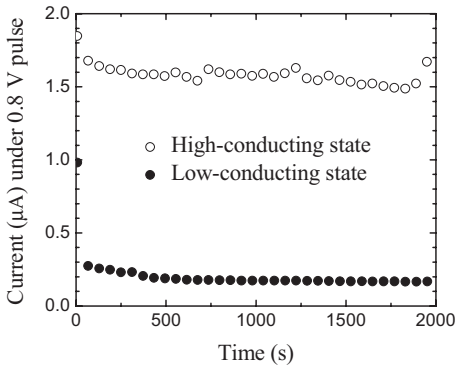

Figure 5. Time response of the low- and high-conducting states of a monolayer. The low and high states were induced by a –0.8 and +0.8 V pulse, respectively. Both the states were probed by a +0.3 V pulse showing the nanoparticles' ability to retain the two conducting states for memory applications.

In conclusion, we have experimentally demonstrated that CdSe nanoparticles with sizes down to the quantum dot regime display electrical bistability. The degree of electrical bistability (on/off ratio) depended on the size of the particles. The two-dimensional array of such particles (via electrostatic assembly) showed conductance switching with an associated memory phenomenon at a suitable voltage. The switching was reversible for many cycles with two sets of *I–V* characteristics. With the scanning tunneling microscope tip as the other electrode, such bistability was observed in a monolayer of the nanoparticles. The results hence demonstrate that CdSe nanoparticles or quantum dots can be used as memory elements with a density of *a bit per particle*.

Experimental

Synthesis: CdSe nanoparticles were synthesized from cadmium acetate ($Cd(COOH)_2.2H_2O$) and sodium selenosulfate (Na_2SeSO_3) following a standard procedure [7,10]. Mercaptoacetic acid was used as a surface–capping agent. Typically, aqueous solutions of cadmium acetate (66.6 mg in 25 mL) and mercaptoacetic acid (15 mg in 20 mL) were mixed thoroughly (pH adjusted by adding dilute NaOH). 2 mL of freshly prepared sodium selenosulfate (prepared by refluxing 2 g of selenium and 4.83 g of sodium sulfite in 100 mL of water for 10 h) was added to the cadmium ion source–mercaptoacetic acid mixed solution. Within 30 min, the transparent solution became greenish yellow and the final product was acid-stabilized CdSe nanoparticles dispersed in water. The pH of the solution containing Cd ions was fixed at 11.5. To achieve CdSe particles with a diameter of 3.5, 4.6, 6.7, and 8.7 nm, the molar ratio of Cd^{2+}/Se^{2-}/mercaptoacetic acid in the reaction mixture was kept at 25:30:13, 23:30:13, 21:30:13, and 17:30:13, respectively. Because the diameter of the particle was of the order of the compound's exciton Bohr radius (around 6 nm) [11], such particles can be termed quantum dots.

The resultant solutions were cooled to 5 °C and centrifuged at 14 000 rpm. The centrifuged powders were dried in a vacuum oven at 60 °C. The acid-stabilized nanoparticles were finally dispersed in deionized water to get an optically homogeneous solution, which was used as an anionic bath for LbL deposition. 5 mM of PAH (M_W = 70,000) solution (pH = 6.5) was used as the cationic bath for LbL film deposition.

ADVANCED MATERIALS

Electrostatic assembly of the nanoparticles: Particles were adsorbed electrostatically on polished Si(111) wafers (arsenic doped, N-type, resistivity = 3–10 mΩ cm) and ITO-coated glass substrates. The substrates were deprotonated in a mixture of H_2O, H_2O_2, and NH_4OH (5:2:2) for 1 h. They were first dipped in the PAH bath for 15 min followed by rinsing in water three times. To obtain a layer of nanoparticles, the PAH-coated substrates were dipped in the disperse solution containing acid-capped CdSe nanoparticles followed by the same rinsing protocol. Electrostatic adsorption of the particles led to a monolayer or a two-dimensional array of CdSe nanoparticles. To record the electronic absorption spectrum, films were deposited on quartz substrates. Multilayers of CdSe, only used to record electronic absorption spectra, were obtained by repeating the PAH and CdSe deposition processes. The films were annealed in vacuum at 100 °C for two days.

Characterization of the nanoparticles: Particles were characterized via XRD and infrared- and UV-vis absorption spectroscopy. The SEM and TEM images of the particles were recorded by using a JEOL JSM-6700 F and JEOL-JEM 2010, respectively.

Electrical characteristics: We recorded the *I–V* characteristics of the two-dimensional array of particles by using a mercury probe and the Pt/Ir tip of a scanning tunneling microscope. Measurements were carried out at room temperature. To characterize the particles with a mercury electrode, the array of nanoparticles was kept in a vacuum chamber (10^{-3} Torr; 1 Torr = 133.322 Pa) with the film facing downward. A syringe with a Hg blob on the tip of a metal needle was raised from outside the chamber slowly by a micrometer screw until the blob just touched the film. The diameter of the blob was below 0.5 mm. The contact between the film and the blob was monitored through a microscope. Bias, applied with respect to the Hg electrode, was swept in both directions and also in loops. For *I–V* measurement through the tip of the scanning tunneling microscope (Nanosurf easyScan 2), bias was scanned before and after application of a suitable voltage pulse. The topographic scanning tunneling microscopy characteristics were recorded with a tip voltage (V_{bias}) of 1.5 V and a tunneling current (I_{ref}) of 0.5 nA, that is, in a constant current mode.

Received: February 5, 2007
Revised: August 6, 2007
Published online: October 30, 2007

[1] V. L. Colvin, M. C. Schlamp, A. P. Alivisatos, *Nature* **1994**, *370*, 354.
[2] X. Duan, Y. Huang, Y. Cui, J. Wang, C. M. Lieber, *Nature* **2001**, *409*, 66.
[3] S. Paul, C. Pearson, A. Molloy, M. A. Cousins, M. Green, S. Kolliopoulou, P. Dimitrakis, P. Normand, D. Tsoukalas, M. C. Petty, *Nano Lett.* **2003**, *3*, 533.
[4] J. Ouyang, C. Chu, C. R. Szmanda, L. Ma, Y. Yang, *Nature Mater.* **2004**, *3*, 918.
[5] M. D. Fischbein, M. Drndic, *Appl. Phys. Lett.* **2005**, *86*, 193 106.
[6] F. Verbakel, S. C. J. Meskers, R. A. J. Janssen, *Appl. Phys. Lett.* **2006**, *89*, 102 103.
[7] K. Mohanta, S. K. Majee, S. K. Batabyal, A. J. Pal, *J. Phys. Chem. B* **2006**, *110*, 18 231.
[8] J. Cho, F. Caruso, *Chem. Mater.* **2005**, *17*, 4547.
[9] D. Lee, M. F. Rubner, R. E. Cohen, *Nano Lett.* **2006**, *6*, 2305.
[10] N. S. Pesika, K. J. Stebe, P. C. Searson, *Adv. Mater.* **2003**, *15*, 1289.
[11] F. W. Wise, *Acc. Chem. Res.* **2000**, *33*, 773.

